

# A Robust and Efficient Boundary Point Detection Method by Measuring Local Direction Dispersion

Dehua Peng, Zhipeng Gui and Huayi Wu

**Abstract**—Boundary points pose a significant challenge for machine learning tasks, including classification, clustering, and dimensionality reduction. Due to the similarity of features, boundary areas can result in mixed-up classes or clusters, leading to a crowding problem in dimensionality reduction. To address this challenge, numerous boundary point detection methods have been developed, but they are insufficiently to accurately and efficiently identify the boundary points in non-convex structures and high-dimensional manifolds. In this work, we propose a robust and efficient method for detecting boundary points using Local Direction Dispersion (LoDD). LoDD considers that internal points are surrounded by neighboring points in all directions, while neighboring points of a boundary point tend to be distributed only in a certain directional range. LoDD adopts a density-independent K-Nearest Neighbors (KNN) method to determine neighboring points, and defines a statistic-based metric using the eigenvalues of the covariance matrix of KNN coordinates to measure the centrality of a query point. We demonstrated the validity of LoDD on five synthetic datasets (2-D and 3-D) and ten real-world benchmarks, and tested its clustering performance by equipping with two typical clustering methods, K-means and Neut. Our results show that LoDD achieves promising and robust detection accuracy in a time-efficient manner.

**Index Terms**—Boundary point detection, clustering, centrality metric, PCA, covariance matrix.

## I. INTRODUCTION

Machine learning plays an essential role in data mining projects, enabling classifications, regression, and revealing key insights through statistical methods or trainable neural network models [1]. The essence of machine learning and deep learning lies in exploring and identifying the aggregation patterns hidden behind data. However, the aggregation patterns of data points can be intricate and indistinct in practical applications due to the irregular shaped structures and complex manifold distributions in feature space [2]. These aggregation patterns typically consist of two parts: internal and boundary points. Internal points are located in the core region of a class, while boundary points straddle two or more classes, defining the class range and extrema. If classes have strong similarities in features, their boundary points can generate mixed-up regions and overlapping patterns, introducing considerable difficulty for machine learning tasks and serving as the primary source of classification error [3].

Boundary points are a critical factor affecting the effectiveness of machine learning methods, and accurate identification of boundary points is necessary. Support Vector Machine (SVM) is a classification algorithm that seeks an optimal decision hyperplane to segregate the data samples [4]. When the data is linearly separable, SVM with a hard margin can easily find a good separator by solving a dual problem with Lagrange multipliers. However, when the classes have noisy or non-linear boundaries, hard-margin SVM must be extended to soft-margin SVM by introducing more constraints based on the primal optimal problem, which can lead to greater errors [5]. Connectivity-based clustering is an important branch of clustering methods that excels in identifying arbitrary shaped clusters. Typically, Density-based Spatial Clustering of Applications with Noise (DBSCAN) leverages circular neighborhoods to connect data points whose densities exceed a threshold [6] and will connect two clusters as a whole if there are continual points at the junction areas between them. Moreover, the boundary points tend to be misidentified as noise due to the low density. Similar situations can occur with grid-based clustering methods, such as WaveCluster [7] and STatistical INformation Grid (STING) [8]. Furthermore, boundary points can result in a crowding problem when it comes to dimensionality reduction. Linear Discriminant Analysis (LDA) is a commonly used predefined step for supervised classification problems [9]. It aims to project data with numerous features into a low-dimensional space with the precondition of maximum separation, but fuzzy class boundaries can make it difficult for LDA to yield an optimal projection plane. As two representative manifold learning methods, t-distributed Stochastic Neighbor Embedding (t-SNE) [10] and Uniform Manifold Approximation and Projection (UMAP) [11], achieve non-linear embedding by approximating the high-dimensional probabilities with Kullback-Leibler (KL) divergence and cross entropy respectively. However, there are often indistinct boundaries between similar classes. To preserve low distance distortion, the classes are likely to become mixed up probably in low-dimensional space, generating an inseparable embedding for subsequent classification methods [12-13].

Actually, there are a number of boundary point detection methods that have been developed, and they can be summarized under two main categories, i.e., density-based and geometry-

Dehua Peng and Huayi Wu are with the State Key Laboratory of Information Engineering in Surveying, Mapping and Remote Sensing, Wuhan University, Wuhan 430079, China, and also with Collaborative Innovation Center of Geospatial Technology, Wuhan University, Wuhan 430079, China. (e-mail: pengdh@whu.edu.cn; wuhuayi@whu.edu.cn).

Zhipeng Gui is with the School of Remote Sensing and Information Engineering, Wuhan University, Wuhan 430079, China, and also with Collaborative Innovation Center of Geospatial Technology, Wuhan University, Wuhan 430079, China. (e-mail: zhipeng.gui@whu.edu.cn).

based methods. Internal points are located in the high-density core regions, while boundary points sit near the margins or free pattern space of the densely distributed classes with a relatively lower density. Considering the density difference, a BOUndaRy points DEtectoR (BORDER) is proposed. It depicts the point density using Reverse K-Nearest Neighbors (RKNN), which identifies the points with a lower RKNN as boundary points [14]. However, it only counts the number of RKNN, but ignores the influence brought by distance between the query point and its neighbors. Border-Peeling Clustering (BPC) designs a density influence factor to detect and peel the boundary points iteratively. It employs Euclidean distance and Gaussian kernel to estimate the combined density influence of RKNN [15]. Instead of an inherent neighborhood parameter in BPC algorithm, Self-Adaptive Neighborhood Border Peeling Clustering (SANBP) uses Natural Nearest Neighbors (NNN) to obtain the neighborhood parameter adaptively, which can generate different neighborhood for each point according to different shapes of the data [16]. Density-based methods have natural defect to handle heterogeneous density, geometry-based methods hence provide another perspective. Based on the intuitive observation that boundary points sit on one side of the class surface, Border-Edge Pattern Selection (BEPS) constructs the approximated tangent hyperplane of a class surface, and measure the directional consistency between the normal vector and vectors formed by the query point and its KNN [17-18]. Similarly, Local Gravitation Clustering (LGC) proposes two metrics, CEnterality (CE) and COordination (CO), to measure the directional consistency between the local attractive forces and mean-shift directions of neighbors [19]. Nonetheless, BEPS and LGC might be invalid for class with non-convex structure. To handle non-convex class, Level Set Boundary Description (LSBD) first fits the data distribution using kernel density estimation dispensing with any assumptions, and then determines the enclosed boundary surface [20]. This prototype-based method is supervised, and requires a time-consuming training process. Besides, an efficient and unsupervised boundary detection algorithm is presented, in which the neighborhood relationships of each point is encoded as a linear data representation in an affine space. The reverse unreachability defined by the number of negative components of the representation matrix, namely  $\mathcal{NC}$ , is exploited to identify the boundary and outlier points [21]. But when the local covariance matrix is not invertible, the representation matrix is unable to be solved. Recently, we propose a novel boundary-seeking clustering algorithm by calculating the local Direction Centrality Metric (DCM) [22]. Its core idea is to measure the uniformity of the directional distribution of KNN. Specifically, DCM is defined as the variance of angles formed by the query point and its KNN in 2-D space, and the variance of simplex volume in higher dimensions. It has strong robustness and adaptability, whereas the calculation of DCM is computationally intensive since the number of simplex increases as dimensions. Therefore, a density-independent boundary point detection method for irregular shaped structures and complex manifolds in high-dimensional space is highly-desired.

In this work, we propose a novel boundary point detection method that builds upon the idea of DCM. The nearest neighbors are distributed relatively uniformly around the internal points, but concentrated in a narrower directional range for a boundary point. Based on this observation, the projection variances of KNN of an internal point would be large and close on all orthogonal axes, while the variances might be small on some directions if the query point is located in the boundary areas. To measure the Local Direction Dispersion (LoDD), we define a centrality metric that utilizes the eigenvalues of the covariance matrix of KNN coordinates after Principal Components Analysis (PCA) rotation. A lower value of the metric indicates a higher likelihood that the query point is a boundary point. We also propose an adaptive method to estimate the number of boundary points. It is capable to determine relatively accurate number of boundary points as long as the data satisfies a weak hypothesis distribution. The validity of LoDD is testified on five synthetic datasets by comparing it with mainstream baselines. LoDD can better cope with the heterogeneous density and weak connectivity, and detect boundary points more accurately on concave structures. We further apply LoDD to clustering tasks by equipping it with two typical clustering techniques, K-means and Ncut. The results show that LoDD can achieve substantial improvement in clustering accuracy on most real-world datasets.

The remainder of this paper is organized as follows. Section II introduces the preliminaries and motivation of our method, and Section III presents the detailed algorithm procedure. Section IV develops an adaptive method for parameter settings. In Section V, we demonstrate the effectiveness on challenging synthetic and real-world datasets and apply it to clustering task. Finally, our conclusions are drawn in Section VI.

## II. PRELIMINARIES AND MOTIVATION

Previous research provides abundant evidence that Direction Centrality Metric (DCM) has a robust performance on different data types and various application scenarios. However, DCM is limited by excessive computational cost on high-dimensional data. This paper intends to follow such a simple and intuitive idea, and evades the computable problem through an alternative calculation strategy. In this section, we first provide a brief review of DCM. Then, we propose a novel centrality metric to measure the local direction dispersion.

### A. Direction Centrality Metric

As described earlier, the uniformity of KNN distribution can indicate the centrality of points. We hence developed DCM for the identification of boundary points in the previous work. An intuitive example of 2-D data is given in Fig. 1, where the number of nearest neighbors (denoted as  $k$ ) is eight. Specifically, we first search the KNN of the current query point and map them onto the unit circle centered at the query point. We do not take the distances of KNN into account. As shown in Fig. 1(a), the eight central angles are approximately equal when the KNN are evenly distributed. While when the KNN are located in a smaller range of direction, like on the positive X axis in Fig. 1(b), angle  $\alpha_5$  is much larger than the other seven angles. Based

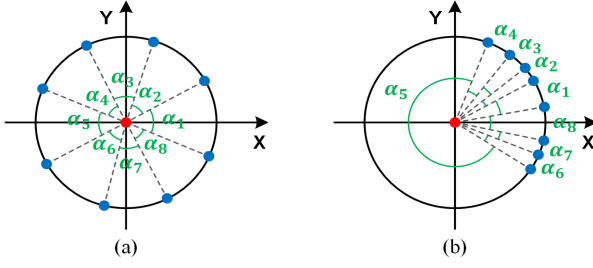


Fig. 1. Illustration of DCM. (a) The angles are approximately equal when KNN are distributed uniformly in the unit circle. (b) The maximum and minimum angles differ a lot when KNN sit in a smaller range of direction.

on this observation, we explicitly define the variance of angles as the direction centrality metric in (1)

$$DCM = \frac{1}{k} \sum_{i=1}^k \left( \alpha_i - \frac{2\pi}{k} \right)^2 \quad (1)$$

where  $\alpha_1, \alpha_2, \dots, \alpha_k$  denote the angles formed by the query point and its KNN, and the condition  $\sum_{i=1}^k \alpha_i = 2\pi$  holds in 2-D space. DCM reaches the minimum 0 if and only if all the angles are equal, which means that the KNN are evenly distributed in all directions. DCM can be maximized as  $\frac{4(k-1)\pi^2}{k^2}$  when one of these angles is  $2\pi$  and the remaining are 0. Such an extreme situation happens when all KNN are distributed in the same direction.

Due to the computable problem of angles, the concept of DCM was extended to include the variance of simplex volumes as dimensions increase. But subsequently, the presence of superabundant simplices results in an extremely high time complexity when calculating DCM in higher dimensions. To address this issue, an auxiliary dimensionality reduction technique is needed to preprocess the raw data [22]. In order to simplify the calculation of DCM in higher dimensions, we redefine it in the following section.

### B. Variance and Centrality

The variances of the coordinates can also reveal the distribution uniformity of KNN, as demonstrated in Fig. 2 using 2-D data. When KNN are uniformly located on the unit circle, the coordinates are dispersed on both axes (Fig. 2(a)). Whereas, when KNN are situated in a smaller range, the coordinates are relatively concentrated on the X axis (Fig. 2(b)).

Nonetheless, the variances of the original coordinates cannot represent the real distribution of KNN directly. When the KNN points are collectively rotated by an angle along the unit circle, their relative positions remain unchanged, but the variance of their coordinates does. Hence, we first use PCA to rotate the KNN in the varimax direction (Fig. 2(c)), and then measure the variances of the coordinates on the rotated axes (Fig. 2(d)). That is because PCA can maximize the difference between the maximum and minimum projection variances. The Principle Components (PCs) are represented by orthogonal lines in the high-dimensional variable space, intersecting at the center of mass of KNN due to the mean-centering process. In PCA, the eigenvalues of the covariance matrix are equal to the variances

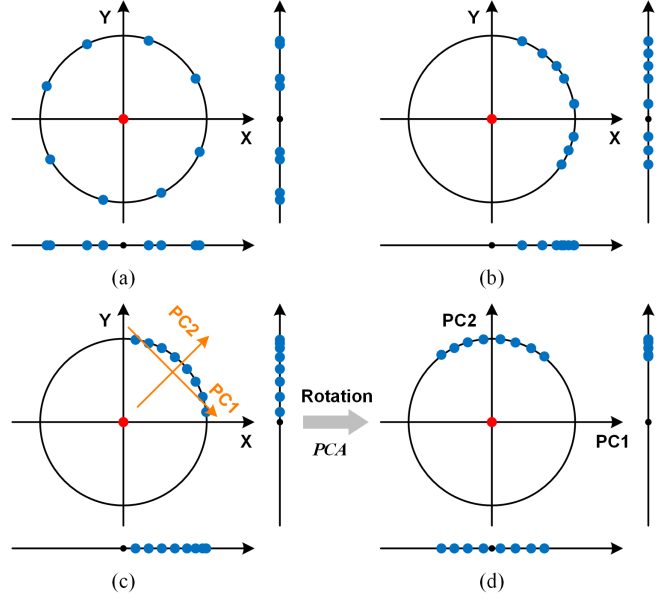


Fig. 2. Illustration of how the variances of the coordinates of KNN indicate the centrality. (a) The case when KNN are distributed uniformly on the unit circle, in which the coordinates are located dispersedly on the axes. (b) The case when KNN are distributed on a smaller range of the unit circle, in which the X coordinates are located compactly on the X axis. (c) Adopting PCA to rotate the original KNN to the varimax direction. (d) The distribution of KNN on the unit circle after PCA rotation as well as their new coordinates.

of the projections in the directions of PCs. In such a scenario, if the variances are larger and more similar, the probability of the query point being a boundary point is lower.

Below, we illustrate the relationship and pattern between KNN projection variances and centrality of the query point through two theorems in 2-D space. Given the coordinates of a query point  $(a_0, b_0)$  and its KNN  $\{(a_1, b_1), (a_2, b_2), \dots, (a_k, b_k)\}$  in 2-D space, we map the KNN onto the unit circle with the center of  $(a_0, b_0)$ , and the coordinates on the unit circle can be calculated as

$$\begin{cases} \hat{a}_i = \frac{a_i - a_0}{\sqrt{(a_i - a_0)^2 + (b_i - b_0)^2}} \\ \hat{b}_i = \frac{b_i - b_0}{\sqrt{(a_i - a_0)^2 + (b_i - b_0)^2}} \end{cases} \quad (2)$$

where  $i$  ranges from 0 to  $k$  and  $(\hat{a}_0, \hat{b}_0) = (0, 0)$ .

We calculate the covariance matrix  $C \in \mathbb{R}^{2 \times 2}$  of  $\{(\hat{a}_1, \hat{b}_1), (\hat{a}_2, \hat{b}_2), \dots, (\hat{a}_k, \hat{b}_k)\}$ , and solve its eigenvalues as  $\lambda_1$  and  $\lambda_2$ . Let the coordinates of KNN after PCA rotation as  $\{(x_1, y_1), (x_2, y_2), \dots, (x_k, y_k)\}$ , then we have

$$\begin{cases} \lambda_1 = \frac{1}{k} \sum_{i=1}^k (x_i - \bar{x})^2 \\ \lambda_2 = \frac{1}{k} \sum_{i=1}^k (y_i - \bar{y})^2 \end{cases} \quad (3)$$

where  $\bar{x} = \frac{1}{k} \sum_{i=1}^k x_i$  and  $\bar{y} = \frac{1}{k} \sum_{i=1}^k y_i$ . It should be noted that we

use population variance ( $1/k$  as coefficient) rather than sample variance ( $1/(k-1)$  as coefficient) in this paper.

*Theorem 1:* When the center of mass of KNN overlaps with the query point,  $\lambda_1 + \lambda_2$  reaches its maximum value of 1; while when the KNN perfectly coincide with each other, both  $\lambda_1$  and  $\lambda_2$  are equal to 0.

*Proof.* We sum up  $\lambda_1$  and  $\lambda_2$

$$\begin{aligned}\lambda_1 + \lambda_2 &= \frac{1}{k} \sum_{i=1}^k (x_i - \bar{x})^2 + \frac{1}{k} \sum_{i=1}^k (y_i - \bar{y})^2 \\ &= \frac{1}{k} \sum x_i^2 - \frac{2\bar{x}}{k} \sum x_i + \bar{x}^2 + \frac{1}{k} \sum y_i^2 - \frac{2\bar{y}}{k} \sum y_i + \bar{y}^2 \\ &= \frac{1}{k} \sum x_i^2 - \bar{x}^2 + \frac{1}{k} \sum y_i^2 - \bar{y}^2\end{aligned}\quad (4)$$

The KNN lie on the unit circle, so the condition  $x_i^2 + y_i^2 = 1$  holds. Then, we can obtain

$$\lambda_1 + \lambda_2 = 1 - \bar{x}^2 - \bar{y}^2 \quad (5)$$

The center of mass of KNN is on or inside the unit circle, that means  $0 \leq \bar{x}^2 + \bar{y}^2 \leq 1$ , so we have

$$0 \leq \lambda_1 + \lambda_2 \leq 1 \quad (6)$$

To some extent,  $\lambda_1 + \lambda_2$  can indicate the symmetry of KNN. Assuming that the gravitational force is acting from the query point towards the KNN, if the resultant force of gravitations is zero, the center of mass of KNN will be located at the query point and  $\bar{x}^2 + \bar{y}^2 = 0$  holds, that means  $\lambda_1 + \lambda_2$  equals 1. On the other hand, when all KNN coincide on the unit circle, the gravitational forces are all acting in the same direction, at this point,  $\bar{x}^2 + \bar{y}^2 = 1$  holds and  $\lambda_1 + \lambda_2$  reaches the minimum value of 0.

*Theorem 2:* If  $k > 2$  and the KNN points are uniformly distributed on the unit circle such that the circle is divided into  $k$  evenly sized arcs, then  $\lambda_1 = \lambda_2 = \frac{1}{2}$ .

*Proof.* When KNN divide the circle into  $k$  equal arcs, the  $k$  central angles formed by the query point and the adjacent KNN are all equal to  $\frac{2\pi}{k}$ .

In this case, suppose the polar coordinates of KNN as  $\{(1, \theta + \frac{2\pi}{k}), (1, \theta + \frac{4\pi}{k}), \dots, (1, \theta + 2\pi)\}$ , then we have

$$\begin{cases} x_i = \cos\left(\theta + \frac{2i\pi}{k}\right) \\ y_i = \sin\left(\theta + \frac{2i\pi}{k}\right) \end{cases} \quad (7)$$

where  $i$  ranges from 1 to  $k$ . We can calculate the X coordinate of the center of mass

$$\begin{aligned}\bar{x} &= \frac{1}{k} \sum_{i=1}^k \cos\left(\theta + \frac{2i\pi}{k}\right) \\ &= \frac{\cos\theta}{k} \sum \cos\left(\frac{2i\pi}{k}\right) - \frac{\sin\theta}{k} \sum \sin\left(\frac{2i\pi}{k}\right)\end{aligned}$$

$$\begin{aligned}&= \frac{\cos\theta}{2k\sin\left(\frac{\pi}{k}\right)} \sum 2\sin\left(\frac{\pi}{k}\right) \cos\left(\frac{2i\pi}{k}\right) - \\ &\quad \frac{\sin\theta}{2k\sin\left(\frac{\pi}{k}\right)} \sum 2\sin\left(\frac{\pi}{k}\right) \sin\left(\frac{2i\pi}{k}\right) \\ &= \frac{\cos\theta}{2k\sin\left(\frac{\pi}{k}\right)} \sum \left( \sin\left(\frac{(2i+1)\pi}{k}\right) - \sin\left(\frac{(2i-1)\pi}{k}\right) \right) - \\ &\quad \frac{\sin\theta}{2k\sin\left(\frac{\pi}{k}\right)} \sum \left( \cos\left(\frac{(2i-1)\pi}{k}\right) - \cos\left(\frac{(2i+1)\pi}{k}\right) \right) \\ &= \frac{\cos\theta}{2k\sin\left(\frac{\pi}{k}\right)} \left( \sin\left(\frac{(2k+1)\pi}{k}\right) - \sin\left(\frac{\pi}{k}\right) \right) - \\ &\quad \frac{\sin\theta}{2k\sin\left(\frac{\pi}{k}\right)} \left( \cos\left(\frac{\pi}{k}\right) - \cos\left(\frac{(2k+1)\pi}{k}\right) \right) = 0\end{aligned}\quad (8)$$

Similarly, we can get  $\bar{y} = 0$ , which means the center of mass of KNN lie on the query point when they form  $k$  equal angles. We can further obtain

$$\begin{aligned}\lambda_1 &= \frac{1}{k} \sum_{i=1}^k (x_i - \bar{x})^2 = \frac{1}{k} \sum_{i=1}^k x_i^2 - \frac{1}{k} \sum_{i=1}^k \cos^2\left(\theta + \frac{2i\pi}{k}\right) \\ &= \frac{1}{2k} \sum \left( 2\cos^2\left(\theta + \frac{2i\pi}{k}\right) - 1 \right) + \frac{1}{2} \\ &= \frac{1}{2k} \sum \left( \cos\left(2\theta + \frac{4i\pi}{k}\right) \right) + \frac{1}{2} \\ &= \frac{\cos 2\theta}{2k} \sum \cos\left(\frac{4i\pi}{k}\right) - \frac{\sin 2\theta}{2k} \sum \sin\left(\frac{4i\pi}{k}\right) + \frac{1}{2} \\ &= \frac{\cos 2\theta}{4k\sin\left(\frac{2\pi}{k}\right)} \sum \left( \sin\left(\frac{(4i+2)\pi}{k}\right) - \sin\left(\frac{(4i-2)\pi}{k}\right) \right) - \\ &\quad \frac{\sin 2\theta}{4k\sin\left(\frac{2\pi}{k}\right)} \sum \left( \cos\left(\frac{(4i-2)\pi}{k}\right) - \cos\left(\frac{(4i+2)\pi}{k}\right) \right) + \frac{1}{2} \\ &= \frac{1}{2}\end{aligned}\quad (9)$$

Given that  $\bar{x} = \bar{y} = 0$ , we can derive  $\lambda_2 = \frac{1}{2}$  using (5).

Relying solely on the symmetrical distribution of KNN on the unit circle is insufficient to guarantee high centrality of the query point. For instance, if half of the KNN are located at  $(1, 0)$  and the other half at  $(-1, 0)$ , we obtain  $\lambda_1 = 1$  and  $\lambda_2 = 0$  using (3). Although the KNN are symmetrically distributed and  $\lambda_1 + \lambda_2$  reaches the maximum value of 1, they do not fill the unit circle and the centrality is not high. According to Theorem 1 and Theorem 2, in order to ensure high centrality of the query point, its KNN not only need to have high symmetry, i.e., the sum of projection variances in each PC, but also requires high spatial dispersion on the unit circle, making the projection variances as close as possible.

### C. Local Direction Dispersion

Based on the analysis above, we can conclude that the sum and proximity of KNN projection variances can be used to assess the centrality of a query point. To account for both factors, we define a centrality metric to measure local direction dispersion for 2-D data

$$\mathcal{L}^{(2)} = \omega(\lambda_1 + \lambda_2) + 4(1 - \omega)\lambda_1\lambda_2 \quad (10)$$

where  $\lambda_1$  and  $\lambda_2$  are the eigenvalues of the covariance matrix of KNN mapped onto the unit circle.  $\omega$  denotes a regulator that controls the respective effects of the sum and closeness of the two variances, and  $0 \leq \omega \leq 1$ .

From (6), we have  $0 \leq \lambda_1 + \lambda_2 \leq 1$ . Moreover,  $\lambda_1\lambda_2$  follows that

$$0 \leq \lambda_1\lambda_2 \leq \frac{(\lambda_1 + \lambda_2)^2}{4} \leq \frac{1}{4} \quad (11)$$

Hence,  $\mathcal{L}^{(2)}$  ranges from 0 to 1, and it can be maximized as 1 if and only if  $\lambda_1 = \lambda_2 = \frac{1}{2}$ ; while it reaches minimum 0 when  $\lambda_1 = \lambda_2 = 0$ .

In  $d$ -dimensional space, Theorem 1 can be generalized

$$\begin{aligned} \sum_{i=1}^d \lambda_i &= \frac{1}{k} \sum_{i=1}^d \sum_{j=1}^k (x_j^{(i)} - \bar{x}^{(i)})^2 \\ &= \sum_i \left( \frac{1}{k} \sum_j x_j^{(i)2} - \frac{2\bar{x}^{(i)}}{k} \sum_j x_j^{(i)} + \bar{x}^{(i)2} \right) \\ &= \frac{1}{k} \sum_j \sum_i x_j^{(i)2} - \sum_i \bar{x}^{(i)2} = 1 - \sum_i \bar{x}^{(i)2} \end{aligned} \quad (12)$$

where  $x_j^{(i)}$  denotes the  $i$ th coordinate of the  $j$ th KNN, and  $\bar{x}^{(i)}$  represents the  $i$ th coordinate of the center of mass.

Meanwhile, we have

$$\sum_{i,j=1, i \neq j}^d \lambda_i \lambda_j = \frac{1}{2} \left( \left( \sum \lambda_i \right)^2 - \sum \lambda_i^2 \right) \leq \frac{1}{2} \left( 1 - \sum \lambda_i^2 \right) \quad (13)$$

With Cauchy's inequality, we have

$$\sum \lambda_i^2 \geq \frac{1}{d} \sum \lambda_i \geq \frac{1}{d} \quad (14)$$

Hence

$$0 \leq \sum_{i,j=1, i \neq j}^d \lambda_i \lambda_j \leq \frac{1}{2} \left( 1 - \sum \lambda_i^2 \right) \leq \frac{d-1}{2d} \quad (15)$$

In conclusion, for  $d$ -dimensional data ( $d \geq 2$ ), we can extend  $\mathcal{L}^{(2)}$  to

$$\mathcal{L}^{(d)} = \omega \sum_{i=1}^d \lambda_i + \frac{2d(1-\omega)}{d-1} \sum_{i,j=1, i \neq j}^d \lambda_i \lambda_j \quad (16)$$

(12) together with (15) yields

$$0 \leq \mathcal{L}^{(d)} \leq 1 \quad (17)$$

Ideally,  $\lambda_1 = \lambda_2 = \dots = \lambda_d = \frac{1}{d}$ ,  $\mathcal{L}^{(d)}$  gets the maximum; while it gets the minimum when all eigenvalues equal to 0.

### III. BOUNDARY POINT DETECTION WITH LOCAL DIRECTION DISPERSION

Based on the centrality metric defined in Section II, we propose a boundary point detection method, namely LoDD. This section describes the overall algorithm procedure and presents a time complexity analysis.

#### A. Algorithm Procedure

The overall workflow of LoDD for detecting boundary points is presented in Algorithm 1. The algorithm takes three input parameters, i.e.,  $\omega$ ,  $k$ , *ratio*, and outputs boundary point set  $\mathbf{X}_B$  and internal point set  $\mathbf{X}_I$  for a point set  $\mathbf{X}$ .  $\omega$  is a regulator that trades off the sum and proximity of projection variances.  $k$  is the parameter of KNN used to determine the number of nearest neighbors, which is commonly relevant to the total number of points, and can be set using an empirical approach [22]. *ratio* denotes the proportion of boundary points in the entire set of points.

In the LoDD procedure, we first search the KNN  $\mathcal{N}(x_i)$  of each query point  $x_i$  in the point set  $\mathbf{X}$ , and then map each KNN point onto the unit circle (or hypersphere). Then, we calculate the covariance matrix of the KNN coordinates as  $\mathbf{C} \in \mathbb{R}^{d \times d}$ . We further conduct eigen-decomposition on  $\mathbf{C}$  and yield  $d$  eigenvalues  $\lambda_1, \lambda_2, \dots, \lambda_d$ . The centrality metric  $\mathcal{L}_i^{(d)}$  of  $x_i$  can be obtained with (16). After calculating the centrality metric of all points in  $\mathbf{X}$ , we sort them in ascending order as  $\tilde{\mathcal{L}}_1^{(d)} \leq \tilde{\mathcal{L}}_2^{(d)} \leq \dots \leq \tilde{\mathcal{L}}_n^{(d)}$ , and specify the threshold as  $\tilde{\mathcal{L}}_{[n \cdot \text{ratio}]}^{(d)}$  using *ratio*. If  $\mathcal{L}_i^{(d)} \leq \tilde{\mathcal{L}}_{[n \cdot \text{ratio}]}^{(d)}$ , then  $x_i$  is detected as a boundary point and added to the set of boundary points  $\mathbf{X}_B$ ; otherwise, it is added to the set of internal points  $\mathbf{X}_I$  as an internal point.

#### B. Time Complexity

To assess the computational efficiency of LoDD, the time complexity of the algorithm is analyzed. Its runtime can be disassembled into four parts:

$$T_{\text{LoDD}} = T_1 + T_2 + T_3 + T_4 \quad (18)$$

where  $T_1, T_2, T_3, T_4$  denote the runtime of KNN search, KNN mapping, and centrality metric calculation and sorting respectively.

KNN can be searched by a brute force method, which is divided into two steps, i.e., distance computation and selecting the  $k$  smallest distances. To be noted, we should consider the number of dimensions  $d$ , since more directions mean longer vectors to compute distances. Hence, the time complexity of  $T_1$  can be represented

$$O(T_1) = O(dn^2 + kn^2) = O((d+k)n^2) \quad (19)$$

---

**Algorithm 1** LoDD for Detecting Boundary Points

---

*Input:*  $\mathbf{X} = \{x_1, x_2, \dots, x_n\} \in \mathbb{R}^{d \times n}$ ,  $\omega, k$ , *ratio*

**for** each point  $x_i \in \mathbf{X}$  **do**

    Search the KNN  $N(x_i) \in \mathbb{R}^{d \times k}$  of  $x_i$

**for** each point  $x_j \in N(x_i)$  **do**

$$x_j \leftarrow \frac{x_j - x_i}{\sqrt{(x_j - x_i)^T (x_j - x_i)}}$$

**end for**

$$\mathbf{C} \leftarrow \left( N(x_i) - \frac{1}{k} \sum_{x_j \in N(x_i)} x_j \right)^T \left( N(x_i) - \frac{1}{k} \sum_{x_j \in N(x_i)} x_j \right)$$

    Obtain eigenvalues  $\lambda_1, \lambda_2, \dots, \lambda_d$  by conducting eigen decomposition on  $\mathbf{C}$

$$\mathcal{L}_i^d \leftarrow \omega \sum \lambda_i + \frac{2d(1-\omega)}{d-1} \sum_{i \neq j} \lambda_i \lambda_j$$

**end for**

Sort  $\mathcal{L}_1^{(d)}, \mathcal{L}_2^{(d)}, \dots, \mathcal{L}_n^{(d)}$  to  $\tilde{\mathcal{L}}_1^{(d)} \leq \tilde{\mathcal{L}}_2^{(d)} \leq \dots \leq \tilde{\mathcal{L}}_n^{(d)}$

**for** each point  $x_i \in \mathbf{X}$  **do**

**if**  $\mathcal{L}_i^{(d)} \leq \tilde{\mathcal{L}}_{[n \cdot \text{ratio}]}^{(d)}$  **do**

$$\mathbf{X}_B \leftarrow \{x_i\}$$

**else do**

$$\mathbf{X}_I \leftarrow \{x_i\}$$

**end if**

**end for**

*Output:*  $\mathbf{X}_B$  and  $\mathbf{X}_I$

---

The time efficiency of KNN search can be improved using k-d tree [23] or ball tree. Both of the two methods have the same time complexity

$$O(T_1) = O(dn \log n + kn \log n) = O((d+k)n \log n) \quad (20)$$

Secondly, the complexity of KNN mapping is

$$O(T_2) = O(kn) \quad (21)$$

Singular Value Decomposition (SVD) algorithm [24] can be employed to factorize the covariance matrix for LoDD calculation, whose time complexity is

$$O(T_3) = O(nd^3) \quad (22)$$

Besides, the average complexity of a commonly-used sort algorithm is  $O(n \log n)$ . In general, the total time complexity of LoDD can be formulated as

$$O(T_{\text{LoDD}}) = O((d+k)n \log n + nd^3) \quad (23)$$

#### IV. ESTIMATION OF THE NUMBER OF BOUNDARY POINTS

Existing boundary detection methods always adopt a threshold for the centrality metric explicitly to distinguish between boundary and internal points [15-17, 20, 22]. However, the threshold varies with data distributions, and it is difficult for users to specify. In comparison, *ratio* has an intuitive physical meaning and is much more stable as data distribution changes [23]. In this section, we propose an adaptive method to estimate the number of boundary points.

##### A. Upper and Lower Bounds

To estimate the upper and lower bounds of the number of boundary points, we introduce a latent grid structure to represent the 2-D data distribution. We provide an example in Fig. 3(a), where a bunch of points can generate an irregular grid by connecting each point with its neighboring points, as shown in Fig. 3(b). We can regularize the structure into a grid composed of unit square cells. In this case, the boundary points are the ones on the periphery of the grid extent, which are denoted as blue points in Fig. 3(c), and their number equals to the periphery length. Actually, a convex grid has the same perimeter as the corresponding Minimum Bounding Rectangle (MBR), since the nonoverlapping outer sides of the grid cells can be projected orthogonally onto the MBR (see the green segments in Fig. 3(d)). Whereas, a concave or ring-shaped grid has a larger perimeter than MBR due to the length of inner segments (see the yellow segments in Fig. 3(e) and (f)). Therefore, the number of boundary points  $\mathcal{B}$  equals to the sum of MBR perimeter and the total length of inner line segments for 2-D data

$$\mathcal{B} = 2(p_1 + p_2 - 2) + l \quad (24)$$

where  $p_1$  and  $p_2$  represent the maximum number of rows and columns of points respectively, and  $l$  denotes the total length of inner line segments. Based on the grid-structure assumption, there are at least two rows or columns of points, and the number of potential points fully-arranged in the MBR with  $p_1$  rows and  $p_2$  columns is greater or equal to the total number  $n$ . Besides, we suppose that  $p_1 \geq p_2$ , thus we have

$$R(p_1, p_2) = \begin{cases} \frac{n}{2} \geq p_1 \geq p_2 \geq 2 \\ p_1 p_2 \geq n \end{cases} \quad (25)$$

Upon the constraint  $R(p_1, p_2)$  in (25), we can yield the upper bound

$$\sup_{R(p_1, p_2)} \mathcal{B} = n \quad (26)$$

$\mathcal{B}$  is smaller than the total number  $n$ , and it reaches the upper bound when  $p_1 = \frac{n}{2}, p_2 = 2$  and  $l = 0$ , that means all points are the boundary points, and the square cells of the grid are arranged in a column under this situation.

Meanwhile, the lower bound follows AM-GM inequality that

$$\inf_{R(p_1, p_2)} \mathcal{B} = 4\sqrt{n} - 4 \quad (27)$$

$\mathcal{B}$  gets the lower bound when  $p_1 = p_2 = \sqrt{n}$ . In this case, the grid is a square with the same number of rows and columns.

The grid-structure assumption is feasible, since it does not rely on the uniformity of data distribution and is robustness with density heterogeneity, and even has no constraints on the shape of point patterns.

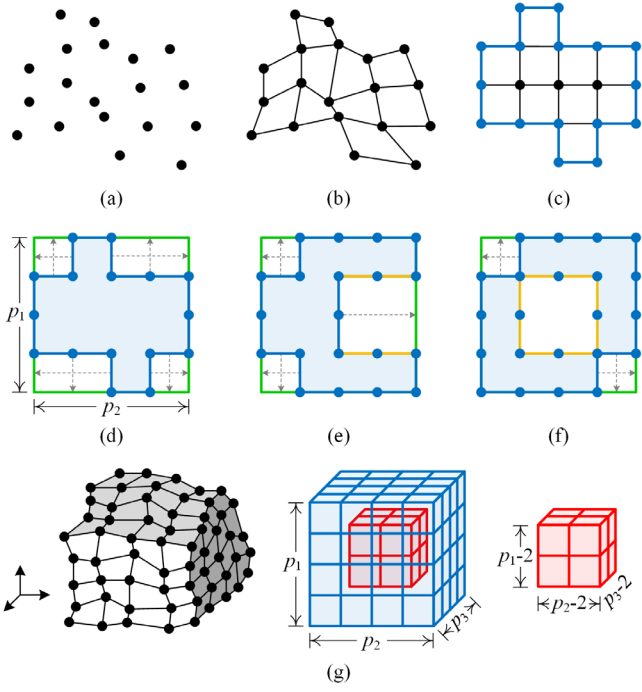


Fig. 3. Estimation of the number of boundary points based on grid-structure assumptions of data distribution. (a) A number of 2-D data points. (b) An irregular grid structure by connecting each point with its neighboring point. (c) A regular grid composed of unit square cells, in which the blue points and lines denote the boundary points and periphery of the grid respectively. (d)-(f) Projecting the nonoverlapping outer sides of the grid cells onto the MBR orthogonally, where the blue areas represent the grid extent, the green and yellow segments denote the orthogonal projections on MBR, and the inner segments of a concave or ring-shaped grid respectively. (g) A 3-D example for estimating the number of boundary points in high-dimensional space, where the boundary points lie on the blue surface and the internal points are in the red hypercuboid.

To estimate the upper and lower bounds of  $\mathcal{B}$  in higher-dimensional space ( $d > 2$ ), we make a stricter assumption that the data can generate an irregular hypercuboid with points fully-arranged in  $p_i$  rows in the  $i$ th dimension latently (see Fig. 3(g)). After converting the cells to regular hypercubes, we know that all the boundary points lie on the outer surface of the hypercuboid. Suppose  $p_1 \geq p_2 \geq \dots \geq p_d$ , then the constraint is

$$R(p_1, p_2, \dots, p_d) = \begin{cases} \frac{n}{2^{d-1}} \geq p_1 \geq p_2 \geq \dots \geq p_d \geq 2 \\ p_1 p_2 \dots p_d = n \end{cases} \quad (28)$$

$\mathcal{B}$  can be obtained by subtracting the number of internal points from the total number of points

$$\mathcal{B} = n - \prod_{i=1}^d (p_i - 2) \quad (29)$$

$\mathcal{B}$  has the same upper bound as in 2-D space

$$\sup_{R(p_1, p_2, \dots, p_d)} \mathcal{B} = n \quad (30)$$

Similarly, it reaches  $n$  when  $p_1 = \frac{n}{2^{d-1}}$  and  $p_2 = p_3 = \dots = p_d = 2$ , which means the data hypercuboid is formed from a number of unit hypercubes arranged in a column.

On the other hand, the objective to calculate the lower bound of (29) is equivalent to

$$\arg \max \prod_{i=1}^d (p_i - 2), s. t. p_1 p_2 \dots p_d = n \quad (31)$$

Using Lagrange multiplier, we construct a function

$$\mathcal{J} = \prod_{i=1}^d (p_i - 2) - \xi (p_1 p_2 \dots p_d - n) \quad (32)$$

Then, we can solve the partial derivative and set them to zero. The system of equations we need to solve is

$$\begin{cases} \frac{\partial \mathcal{J}}{\partial \xi} = n - p_1 p_2 \dots p_d = 0 \\ \frac{\partial \mathcal{J}}{\partial p_i} = \prod_{j \neq i} (p_j - 2) - \xi \prod_{j \neq i} p_j = 0 \end{cases} \quad (33)$$

By solving (33), we have

$$p_1 = p_2 = \dots = p_d = \sqrt[d]{n} \quad (34)$$

It follows from (29) and (34) that

$$\inf_{R(p_1, p_2, \dots, p_d)} \mathcal{B} = n - (\sqrt[d]{n} - 2)^d \quad (35)$$

Based on the grid-structure assumption of data distribution, we can estimate an approximate range of  $\mathcal{B}$

$$n - (\sqrt[d]{n} - 2)^d \leq \mathcal{B} \leq n \quad (36)$$

### B. Determination of ratio

The number of boundary points  $\mathcal{B}$  in a point pattern can be estimated using (36). However, there are usually more than one class or cluster in the data. Thus, we need to obtain a rough estimate of the number of points in each class or cluster before determining *ratio*.

If the exact number of classes  $c$  is known in advance, we can roughly assume that each class has the same number of points. In this case, *ratio* can be determined using the lower bound of  $\mathcal{B}$  in (35)

$$ratio = \frac{\mathcal{B}}{n} = 1 - \frac{(\sqrt[d]{n} - 2\sqrt[d]{c})^d}{n} \quad (37)$$

If  $c$  is unknown, we can construct a KNN graph, and the number of points in each generated connected component can be considered as a rough estimate of the true number of points of each class. The construction of KNN graph can be performed simultaneously with KNN searching in the LoDD algorithm, which does not introduce excessive extra time cost. Suppose the KNN graph consists of  $m$  connected components, with  $n_1, n_2, \dots, n_m$  points respectively, then we can determine the *ratio* as

$$ratio = \frac{\mathcal{B}}{n} = 1 - \frac{\sum_{i=1}^m (\sqrt[d]{n_i} - 2)^d}{n} \quad (38)$$

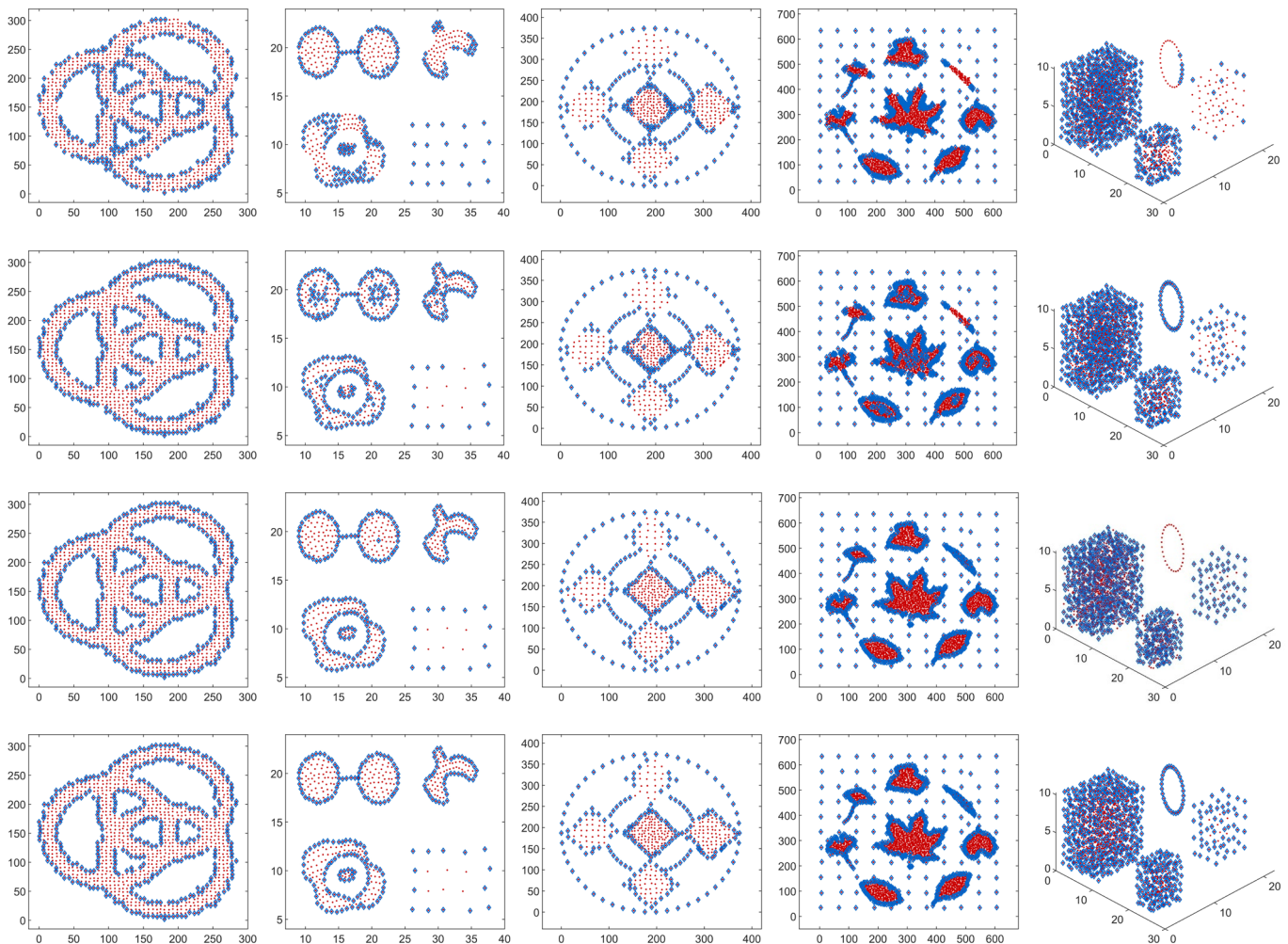


Fig. 4. Boundary points detected by four methods on five synthetic datasets (DS1-DS5), where the four rows represent the results of LGC, BORDER, DCM and LoDD respectively. The blue diamonds denote the boundary points, while the red points refer to the internal points.

## V. EXPERIMENTAL RESULTS

### A. Validation on synthetic datasets

To validate the accuracy of boundary detection, we compared the LoDD algorithm with three baselines: LGC [19], a geometry-based method; BORDER [14], a density-based method; and DCM [22], on five synthetic datasets by measuring the consistency between the detected results and true labels using F1-score. These challenging datasets include four 2-D point sets (DS1-DS4) and one 3-D point set (DS5).

*Parameter settings:* All the four centrality metrics, i.e., RNN in BORDER, CE in LGC, DCM, and  $\mathcal{L}$  in LoDD, are KNN-based. We vary  $k$  in the same range from 5 to 30 with an interval of 1 for all methods. The four metrics of all points are sorted in ascending order respectively. Then, the metric value of the  $[n \cdot \text{ratio}]$ th point is used as the threshold to distinguish between boundary and internal points. We manually label the boundary points in the five synthetic datasets, and specify the *ratio* as the proportion of true boundary points in all points. We also

perform LoDD using *ratio* adaptively obtained from (37), denoted as aLoDD. The initial momentum of LGC is set to 10, and the regulator  $\omega$  in LoDD is fixed at 0.5.

*Results:* Detection results that correspond the max F1-score are illustrated in Fig. 4, and the max and mean F1-score are presented in Fig. 5. In general, LoDD using both the optimal and adaptive *ratio* (aLoDD) outperforms LGC and BORDER both in max and mean F1-score on all datasets. LoDD has similar performance in max F1-score with DCM in 2-D space, and distinct advantage on the 3-D dataset. Due to the uniform density in DS1, all the methods obtain promising results with a max F1-score higher than 0.8. However, LoDD and DCM challenging datasets, with clusters distributed with huge density differences, weak connectivity, and island structures. LGC detects all points belonging to the low-density cluster in DS2 as boundary points, since the CE metric relies on mean-shift directions. While, LoDD can accurately seek out the boundary points of weakly-connected and sparse clusters. aLoDD even achieves higher accuracy than LoDD on DS3. DS4 includes background noise behind the dense leaf-shaped clusters. The



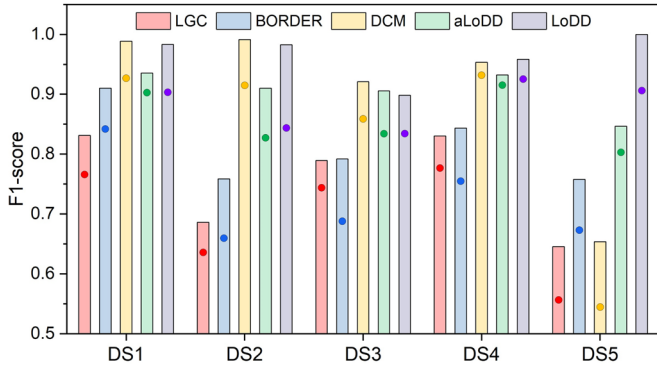


Fig. 5. The max and mean F1-score of the four boundary detection methods by varying  $k$  on five synthetic datasets, where the color bar and circle denote the max and mean F1-scores respectively.

boundary points detected by LGC are incomplete, and BORDER tends to discern partial internal points with low local density as boundary points. In comparison, LoDD is robust to the noise and is able to outline the periphery of each cluster, and yields a higher max F1-score than DCM. DS5 is composed of a circle manifold and three cube-shaped clusters with different densities. The boundary points of the sparse cluster and circle manifold have not been fully explored by LGC, and BORDER detects excess boundary points for the two dense cubes, and DCM misses the boundary points in the circle manifold. By contrast, LoDD identifies the boundary points in a precise and complete manner, and achieves a F1-score of 1.

### B. Clustering performance

Boundary detection methods have positive impact on clustering quality, and in turn, the clustering accuracy can implicitly reflect the effectiveness of boundary detection. To verify the performance on high-dimensional data, we equip K-means [25] and Normalized cut (Ncut) [26] algorithms with boundary detectors, and apply them on ten real-world datasets. We investigate a density-based and geometry-based boundary detector for comparing with our method, i.e., BPC [15] and  $\mathcal{NC}$  [21] respectively, both of which have been applied to clustering tasks. As mentioned in Introduction Section, misclassification of boundary points is one of the major factors affecting clustering accuracy. Hence, we first identify and pick out the boundary points, and then cluster the internal points. Finally, we assign the cluster label of the nearest internal point to each boundary point.

*Datasets:* Ten real-world datasets are collected for the clustering performance experiment, and their detailed information is presented in Table 1. Iris, Vehicle, Breast and Mice are four UCI datasets [27] with features scaled to  $[0, 1]$  using min-max normalization, i.e.,  $f_i = (f_i - f_{min}) / (f_{max} - f_{min})$ . Digits and MNIST10k [28] are two typical handwritten digit images with size of  $8 \times 8$  and  $28 \times 28$  respectively. They are converted to 1-D vectors from 2-D image matrices before clustering. Yale contains totally 165 face images with size of  $64 \times 64$  from 15 distinct individuals [29]. We extract the Gabor, Gist and LBP image features from Yale, and then perform Principal Component Analysis (PCA) [30] to embed the three

TABLE I  
INFORMATION OF TEN REAL-WORLD DATASETS

Dataset	Description	Instances	Dimensions	Classes
Iris	UCI	150	4	3
Vehicle	UCI	846	18	4
Breast	UCI	683	10	2
Mice	UCI	1,077	77	8
Digits	Handwritten Digits	5,620	$8 \times 8$	10
MNIST10k	Handwritten Digits	10,000	$28 \times 28$	10
Yale	Face Images	165	$64 \times 64$	15
TDT2-5	Text Documents	2,173	36,771	5
TDT2-10	Text Documents	4,315	36,771	10
Reuters	Text Documents	8,293	18,933	65

features individually in 25 dimensions. Finally, we concatenate the embedded features and feed them to the clustering procedure. TDT2-5 and TDT2-10 are two subsets of the original TDT2 document dataset, which have 5 and 10 semantic categories respectively [31]. Reuters corpus contains 8,293 documents in 65 categories. For the three text documents, we yield the Term Frequency-Inverse Document Frequency (TF-IDF) [32] of each word, and the TF-IDF features are embedded in 100 dimensions by PCA.

*Evaluation metrics:* We exploit ACCuracy (ACC) and F1-score metrics to evaluate the clustering quality. ACC refers to the accuracy rate of the clustering results compared with the true labels. We set the true label vector and the predicted label vector as  $t = (t_1, t_2, \dots, t_n) \in \mathbb{R}^n$  and  $r = (r_1, r_2, \dots, r_n) \in \mathbb{R}^n$  respectively, and the ACC can be calculated as

$$ACC(t, r) = \frac{\sum_{i=1}^n \delta(t_i, \text{map}(r_i))}{n} \quad (39)$$

where  $\delta(\cdot)$  denotes an indicator function

$$\delta(x, y) = \begin{cases} 1 & \text{if } x = y \\ 0 & \text{otherwise} \end{cases} \quad (40)$$

$\text{map}(\cdot)$  is a mapping function that maps each predicted label to one of the true cluster labels. Commonly, the best mapping can be found by using the Kuhn-Munkres or Hungarian algorithms.

*Experimental settings:* K-means requires determining the initial cluster centers, which affects the convergence speed and clustering accuracy. We borrow the idea from density peak clustering algorithm [33], which suggests that the cluster centers tend to have high local density and are far from other cluster centers. The local *density* is defined as the number of points within the cutoff distance, where the cutoff distance is determined as the 5th percentile Euclidean distance among all point pairs in ascending order. *minDis* denotes the minimum distance between the current point and any other point with higher *density*. We normalize *density* and *minDis* of each point to  $[0, 1]$ , and calculate a score

$$\text{score} = 0.5(\text{density} + \text{minDis}) \quad (41)$$

The first  $c$  ( $c$  denotes the number of clusters) points having the largest *score* are selected as the initial cluster centers of K-means. Both K-means and Ncut need to input  $c$ , which is

TABLE II  
THE AVERAGE ACC ( $\pm$ STANDARD DEVIATION) ON TEN REAL-WORLD DATASETS  
(THE BEST RESULT OF EACH DATASET IS HIGHLIGHTED IN BOLD)

Datasets	<i>K-means</i>				<i>Ncut</i>			
	Original	BPC	<i>NC</i>	LoDD	Original	BPC	<i>NC</i>	LoDD
Iris	0.5714	0.6158( $\pm$ 0.164)	0.6452( $\pm$ 0.181)	<b>0.6751(<math>\pm</math>0.182)</b>	0.8776	0.8729( $\pm$ 0.075)	0.8735( $\pm$ 0.073)	<b>0.8865(<math>\pm</math>0.006)</b>
Breast	0.9615	0.9578( $\pm$ 0.001)	0.9573( $\pm$ 0.002)	<b>0.9621(<math>\pm</math>0.004)</b>	0.9496	0.9627( $\pm$ 0.002)	0.9644( $\pm$ 0.002)	<b>0.9665(<math>\pm</math>0.002)</b>
Vehicle	0.3842	<b>0.3862(<math>\pm</math>0.004)</b>	0.3858( $\pm$ 0.003)	0.3859( $\pm$ 0.008)	0.3723	0.3749( $\pm$ 0.005)	0.3775( $\pm$ 0.005)	<b>0.3873(<math>\pm</math>0.006)</b>
Mice	0.3473	0.3614( $\pm$ 0.021)	0.3524( $\pm$ 0.021)	<b>0.3675(<math>\pm</math>0.015)</b>	0.3203	0.3225( $\pm$ 0.014)	<b>0.3286(<math>\pm</math>0.012)</b>	0.3238( $\pm$ 0.021)
Digits	0.6680	0.7506( $\pm$ 0.036)	0.7495( $\pm$ 0.054)	<b>0.7658(<math>\pm</math>0.037)</b>	0.7137	0.7719( $\pm$ 0.057)	0.7759( $\pm$ 0.055)	<b>0.7910(<math>\pm</math>0.038)</b>
MNIST10k	0.5290	0.5696( $\pm$ 0.037)	0.5653( $\pm$ 0.040)	<b>0.5784(<math>\pm</math>0.028)</b>	0.4543	0.4680( $\pm$ 0.020)	0.4663( $\pm$ 0.014)	<b>0.4724(<math>\pm</math>0.014)</b>
Yale	0.5337	0.5205( $\pm$ 0.051)	0.5283( $\pm$ 0.034)	<b>0.5541(<math>\pm</math>0.048)</b>	0.6012	0.6160( $\pm$ 0.051)	0.5855( $\pm$ 0.061)	<b>0.6528(<math>\pm</math>0.041)</b>
TDT2-5	0.3107	0.4040( $\pm$ 0.040)	0.4187( $\pm$ 0.060)	<b>0.4663(<math>\pm</math>0.091)</b>	0.5767	0.5871( $\pm$ 0.009)	0.5751( $\pm$ 0.011)	<b>0.5948(<math>\pm</math>0.073)</b>
TDT2-10	0.5064	0.5964( $\pm$ 0.046)	0.5789( $\pm$ 0.037)	<b>0.5976(<math>\pm</math>0.039)</b>	0.6284	0.6522( $\pm$ 0.045)	0.6358( $\pm$ 0.061)	<b>0.6541(<math>\pm</math>0.052)</b>
Reuters	0.1978	0.2274( $\pm$ 0.015)	0.2215( $\pm$ 0.015)	<b>0.2596(<math>\pm</math>0.024)</b>	0.1902	0.1999( $\pm$ 0.011)	0.1913( $\pm$ 0.012)	<b>0.2070(<math>\pm</math>0.017)</b>

TABLE III  
THE AVERAGE F1-score ( $\pm$ STANDARD DEVIATION) ON TEN REAL-WORLD DATASETS  
(THE BEST RESULT OF EACH DATASET IS HIGHLIGHTED IN BOLD)

Datasets	<i>K-means</i>				<i>Ncut</i>			
	Original	BPC	<i>NC</i>	LoDD	Original	BPC	<i>NC</i>	LoDD
Iris	0.6501	0.7011( $\pm$ 0.075)	0.7171( $\pm$ 0.082)	<b>0.7201(<math>\pm</math>0.082)</b>	0.7955	0.8042( $\pm$ 0.034)	0.8043( $\pm$ 0.035)	<b>0.8086(<math>\pm</math>0.009)</b>
Breast	0.9323	0.9262( $\pm$ 0.002)	0.9256( $\pm$ 0.003)	<b>0.9333(<math>\pm</math>0.004)</b>	0.9134	0.9339( $\pm$ 0.004)	0.9370( $\pm$ 0.004)	<b>0.9402(<math>\pm</math>0.003)</b>
Vehicle	0.3363	<b>0.3342(<math>\pm</math>0.009)</b>	0.3333( $\pm$ 0.007)	0.3315( $\pm$ 0.008)	0.2964	0.3014( $\pm$ 0.005)	0.3032( $\pm$ 0.003)	<b>0.3081(<math>\pm</math>0.004)</b>
Mice	0.3030	0.3110( $\pm$ 0.020)	0.3051( $\pm$ 0.013)	<b>0.3121(<math>\pm</math>0.010)</b>	0.2504	<b>0.2637(<math>\pm</math>0.018)</b>	0.2576( $\pm$ 0.011)	0.2578( $\pm$ 0.016)
Digits	0.6284	0.6850( $\pm$ 0.030)	0.6849( $\pm$ 0.039)	<b>0.6984(<math>\pm</math>0.030)</b>	0.6304	0.6960( $\pm$ 0.048)	0.6996( $\pm$ 0.044)	<b>0.7056(<math>\pm</math>0.030)</b>
MNIST10k	0.3986	0.4479( $\pm$ 0.028)	0.4467( $\pm$ 0.028)	<b>0.4506(<math>\pm</math>0.013)</b>	0.3861	0.3918( $\pm$ 0.009)	0.3895( $\pm$ 0.007)	<b>0.3945(<math>\pm</math>0.007)</b>
Yale	0.4068	0.3916( $\pm$ 0.043)	0.3931( $\pm$ 0.032)	<b>0.4166(<math>\pm</math>0.043)</b>	0.4179	0.4410( $\pm$ 0.049)	0.4140( $\pm$ 0.060)	<b>0.4531(<math>\pm</math>0.048)</b>
TDT2-5	0.4178	0.4801( $\pm$ 0.052)	0.4498( $\pm$ 0.038)	<b>0.5287(<math>\pm</math>0.062)</b>	0.6494	0.6582( $\pm$ 0.008)	0.6569( $\pm$ 0.008)	<b>0.6658(<math>\pm</math>0.007)</b>
TDT2-10	0.5395	<b>0.6029(<math>\pm</math>0.042)</b>	0.5846( $\pm$ 0.031)	0.5915( $\pm$ 0.035)	0.5808	<b>0.6228(<math>\pm</math>0.044)</b>	0.5956( $\pm$ 0.075)	0.5929( $\pm$ 0.051)
Reuters	0.1192	0.1511( $\pm$ 0.015)	0.1429( $\pm$ 0.015)	<b>0.1674(<math>\pm</math>0.023)</b>	0.1075	0.1213( $\pm$ 0.009)	0.1094( $\pm$ 0.010)	<b>0.1222(<math>\pm</math>0.012)</b>

specified as the true number of clusters of each dataset. We set  $k$  from 10 to 30 with an interval of 5, and  $ratio$  from 0.1 to 0.3 with an interval of 0.05, for BPC,  $NC$  and LoDD.

*Results:* We compare the performance of the original clustering algorithms and those equipped with three boundary detectors. The mean and standard deviation of ACC and F1-score are presented in Table 2 and 3. In general, K-means and Ncut equipped with boundary detectors can improve clustering accuracy, and LoDD has the greatest improvement than the competitors. By integrating LoDD, K-means achieves the highest average ACC and F1-score on nine and eight datasets respectively. Significant improvements are observed on Iris, Digits, MNIST10k, TDT2-5, TDT2-10 and Reuters, where the average ACC and F1-score improvements surpass 0.04 compared to the original version. Ncut equipped with LoDD also obtains the highest average ACC and F1-score on nine and eight datasets respectively, outperforming BPC and  $NC$  by a large margin. The three boundary detectors show similar robustness to the parameters in terms of the standard deviation. Overall, the results demonstrate that LoDD can achieve better identification accuracy of boundary points in high-dimensional space, and integrating LoDD with K-means and Ncut can significantly improve clustering accuracy across various real-world datasets.

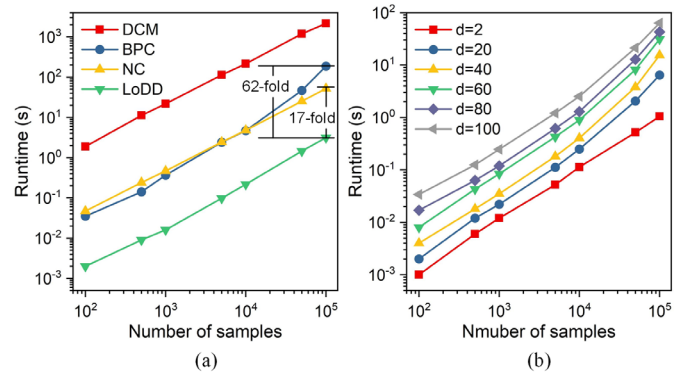


Fig. 6. Time efficiency analysis for LoDD. (a) Runtimes of four boundary detection methods on 10-D simulated datasets with different number of samples. (b) Runtimes of LoDD on simulated datasets with different number of dimensions and samples.

### C. Time efficiency analysis

The time efficiency analysis is conducted on a commodity desktop computer with 12-core Intel i7 processor and 32 GB RAM. All the methods are implemented in MATLAB R2022a, and the average runtimes are measured by varying the  $k$  of KNN from 10 to 30 with an interval of 5. Fig. 6(a) shows the runtime comparison between LoDD and three mainstream boundary detectors on simulated datasets with ten dimensions and different data sizes. LoDD is found to be more efficient than the competitors, running around 17-fold faster than  $NC$ , 62-fold

faster than BPC, and 700-fold faster than DCM on the 10-D dataset with 105 samples. Fig. 6(b) illustrates that the time efficiency of LoDD is also related to the data dimension and has the polynomial complexity as dimensionality increases, which coincides with the time complexity analysis in Section III. Additionally, LoDD embraces parallel computing and is GPU-friendly because the centrality metric calculation of each point is independent of each other. It can be easily extended to parallel versions using GPGPU and distributed computing techniques such as Apache Spark for performance acceleration [34].

## VI. CONCLUSION

This paper proposes a robust boundary point detection method by measuring Local Direction Dispersion (LoDD). It inherits the idea of DCM, which considers the distribution uniformity of local nearest neighbors, but redefines the centrality metric using the projection variances on PCs. Additionally, we develop an adaptive method to estimate the number of boundary points, which facilitates parameter specification. Compared with related methods, both LoDD and aLoDD outperform LGC and BORDER on synthetic datasets. When applied to clustering tasks, LoDD generates larger improvements in clustering accuracy than BPC and  $\mathcal{NC}$  on multiple data types. The time efficiency is further analyzed on simulated datasets of various sizes, and the results indicate that LoDD runs substantially faster than the competitors. Although LoDD follow the idea of DCM, the redefinition of centrality metric makes LoDD yield similar detection accuracy with DCM but with significantly higher efficiency especially in higher dimensions. In a sense, this modification extends the applied areas for DCM. In general, LoDD is a robust and efficient boundary point detector, and can provide prior knowledge and constraints of data distribution to benefit various machine learning tasks.

## REFERENCES

- [1] P. P. Shinde and S. Shah, "A Review of Machine Learning and Deep Learning Applications," in *Proc. 4th ICCUBEA*, Pune, India, 2018, pp. 1-6.
- [2] Z. Gui, D. Peng, H. Wu and X. Long, "MSGC: multi-scale grid clustering by fusing analytical granularity and visual cognition for detecting hierarchical spatial patterns," *Future Gener. Comput. Syst.*, vol. 112, pp. 1038-1056, Nov. 2020.
- [3] R. Barandela, F. J. Ferri, and J. S. Sanchez, "Decision Boundary Preserving Prototype Selection for Nearest Neighbour Classification," *Intern. J. Pattern Recognit. Artif. Intell.*, vol. 19, no. 6, pp. 787-806, Sep. 2005.
- [4] V. N. Vapnik, *The Nature of Statistical Learning Theory*. Springer-Verlag, New York, 1995.
- [5] M. Huang and L. Carvalho, "Soft-SVM Regression For Binary Classification," 2022, *arXiv:2205.11735*.
- [6] M. Ester, H.-P. Kriegel, J. Sander and X. Xu, "A density-based algorithm for discovering clusters in large spatial databases with noise," in *Proc. 2nd Int. Conf. Knowl. Discovery Data Mining*, 1996, vol. 96, no. 34, pp. 226-231.
- [7] G. Sheikholeslami, S. Chatterjee, and A. Zhang, "WaveCluster: A Multi-Resolution Clustering Approach for Very Large Spatial Databases," in *Proc. 23rd Intl. Conf. on Very Large Data Bases (VLDB)*, 1998, pp. 428-439.
- [8] W. Wang, J. Yang, and R. Muntz, "STING: A Statistical Information Grid Approach to Spatial Data Mining," in *Proc. 23rd Intl. Conf. on Very Large Data Bases (VLDB)*, 1997, pp. 186-195.
- [9] K. Fukunaga, *Introduction to Statistical Pattern Recognition*, 2nd ed. San Diego, CA: Academic, 1990.
- [10] L. van der Maaten, and G. Hinton, "Visualizing data using t-SNE," *J. Mach. Learn. Res.* vol. 9, no. 86, pp. 2579-2605, 2008.
- [11] L. McInnes, J. Healy, N. Saul and L. Grobberger, "UMAP: Uniform Manifold Approximation and Projection," *J. Open Source Softw.* vol. 3, no. 29, pp. 861, Sep. 2018.
- [12] Z. Yang, Y. Chen and J. Corander, "T-SNE Is Not Optimized to Reveal Clusters in Data," 2021, *arXiv:2110.02573*.
- [13] Z. Zhou, X. Zu, Y. Wang, B. P. F. Lelieveldt and Q. Tao, "Deep Recursive Embedding for High-Dimensional Data," *IEEE Trans. Vis. Comput. Graph.* vol. 28, no. 2, pp. 1237-1248, Feb. 2022.
- [14] C. Xia, W. Hsu, M. L. Lee and B. C. Ooi, "BORDER: efficient computation of boundary points," *IEEE Trans. Knowl. Data Eng.*, vol. 18, no. 3, pp. 289-303, Mar. 2006.
- [15] H. Averbuch-Elor, N. Bar and D. Cohen-Or, "Border-Peeling Clustering," *IEEE Trans. Pattern Anal. Mach. Intell.*, vol. 42, no. 7, pp. 1791-1797, Jul. 2020.
- [16] J. Feng, B. Zhang, R. Ran, W. Zhang and D. Yang, "An Effective Clustering Algorithm Using Adaptive Neighborhood and Border Peeling Method," *Comput. Intell. Neurosci.*, vol. 2021, Nov. 2021.
- [17] Y. Li and L. Maguire, "Selecting Critical Patterns Based on Local Geometrical and Statistical Information," *IEEE Trans. Pattern Anal. Mach. Intell.*, vol. 33, no. 6, pp. 1189-1201, Jun. 2011.
- [18] Y. Li, "Selecting training points for one-class support vector machines," *Pattern Recognit. Lett.*, vol. 32, no. 11, pp. 1517-1522, Aug. 2011.
- [19] Z. Wang, Z. Yu, C. L. P. Chen, J. You, T. Gu, H.-S. Wong and J. Zhang, "Clustering by Local Gravitation," *IEEE Trans. Cybern.*, vol. 48, no. 5, pp. 1383-1396, May 2018.
- [20] X. Ding, Y. Li, A. Belatreche and L. P. Maguire, "Novelty Detection Using Level Set Methods," *IEEE Trans. Neural Netw. Learn. Syst.*, vol. 26, no. 3, pp. 576-588, Mar. 2015.
- [21] X. Li, J. Lv and Z. Yi, "An Efficient Representation-Based Method for Boundary Point and Outlier Detection," *IEEE Trans. Neural Netw. Learn. Syst.*, vol. 29, no. 1, pp. 51-62, Jan. 2018.
- [22] D. Peng, Z. Gui, D. Wang, Y. Ma, Z. Huang, Y. Zhou and H. Wu, "Clustering by measuring local direction centrality for data with heterogeneous density and weak connectivity," *Nat. Commun.* vol. 13, pp. 5455, Sep. 2022.
- [23] J. L. Bentley, "Multidimensional binary search trees used for associative searching," *Commun. ACM* vol. 18, no. 9, pp. 509-517, Sept. 1975.
- [24] M. Moonen and B. de Moor, *SVD and Signal Processing III*. Elsevier, New York, 1995.
- [25] M. Su and C. Chou, "A modified version of the k-means algorithm with a distance based on cluster symmetry," *IEEE Trans. Pattern Anal. Mach. Intell.*, vol. 23, no. 6, pp. 674-680, Jun. 2001.
- [26] J. Shi and J. Malik, "Normalized cuts and image segmentation," *IEEE Trans. Pattern Anal. Mach. Intell.*, vol. 22, no. 8, pp. 888-905, Aug. 2000.
- [27] D. Dua and C. Graff, "UCI machine learning repository," 2019, [Online]. Available: <http://archive.ics.uci.edu/ml>.
- [28] Y. Lecun, L. Bottou, Y. Bengio and P. Haffner, "Gradient-based learning applied to document recognition," *Proc. IEEE*, vol. 86, no. 11, pp. 2278-2324, Nov. 1998.
- [29] K.-C. Lee, J. Ho, and D. Kriegman, "Acquiring Linear Subspaces for Face Recognition under Variable Lighting," *IEEE Trans. Pattern Anal. Mach. Intell.*, vol. 27, no. 5, pp. 684-698, May 2005.
- [30] H. Hotelling, "Analysis of a complex of statistical variables into principal components," *J. Educ. Psychol.* vol. 24, no. 6, pp. 417-441, 1933.
- [31] D. Cai, X. He and J. Han, "Document clustering using locality preserving indexing," *IEEE Trans. Knowl. Data Eng.*, vol. 17, no. 12, pp. 1624-1637, Dec. 2005.
- [32] K. S. Jones, "A statistical interpretation of term specificity and its application in retrieval," *J. Doc.*, vol. 28, no. 1, pp. 11-21, Jan. 1972.
- [33] A. Rodriguez and A. Laio, "Clustering by fast search and find of density peaks," *Science*, vol. 344, no. 6191, pp. 1492-1496, Jun. 2014.
- [34] Y. Wang, Z. Gui, H. Wu, D. Peng, J. Wu and Z. Cui, "Optimizing and accelerating space-time Ripley's K function based on Apache Spark for distributed spatiotemporal point pattern analysis," *Future Gener. Comput. Syst.*, vol. 105, pp. 96-118, Apr. 2020.